Nuclear Instruments and Methods in Physics Research B 362 (2015) 38–44

Contents lists available at ScienceDirect

Nuclear Instruments and Methods in Physics Research B

journal homepage: www.elsevier.com/locate/nimb

Determination of the effective sample thickness via radiative capture

A.M. Hurst [a,*], N.C. Summers [b], L. Szentmiklósi [c], R.B. Firestone [a], M.S. Basunia [a], J.E. Escher [b], B.W. Sleaford [b]

[a] Lawrence Berkeley National Laboratory, Berkeley, CA 94720, USA
[b] Lawrence Livermore National Laboratory, Livermore, CA 94550, USA
[c] Centre for Energy Research, Hungarian Academy of Sciences, H-1525 Budapest, Hungary

ARTICLE INFO

Article history:
Received 24 June 2015
Received in revised form 18 August 2015
Accepted 1 September 2015

Keywords:
Prompt Gamma Activation Analysis (PGAA)
γ-Ray absorption
Neutron attenuation
(n, γ) radiative capture
Partial γ-ray production cross sections

ABSTRACT

A procedure for determining the effective thickness of non-uniform irregular-shaped samples via radiative capture is described. In this technique, partial γ-ray production cross sections of a compound nucleus produced in a neutron-capture reaction are measured using Prompt Gamma Activation Analysis and compared to their corresponding standardized absolute values. For the low-energy transitions, the measured cross sections are lower than their standard values due to significant photoelectric absorption of the γ rays within the bulk-sample volume itself. Using standard theoretical techniques, the amount of γ-ray self absorption and neutron self shielding can then be calculated by iteratively varying the sample thickness until the observed cross sections converge with the known standards. The overall attenuation, thus, provides a measure of the effective sample thickness illuminated by the neutron beam. This procedure is illustrated through radiative neutron capture using powdered oxide samples comprising enriched ^{186}W and ^{182}W from which their tungsten-equivalent effective thicknesses are deduced to be 0.077(3) mm and 0.042(8) mm, respectively.

1. Introduction

For accurate nuclear-data measurements, targets with well-defined geometries, thicknesses, homogeneities and compositions (e.g. thin metal foils and pellets) are preferred. In many cases, however, this ideal case cannot be achieved and there are several applications of in-beam measurements where the irradiated sample may take an irregular inhomogeneous form. For irradiated powders in particular, the material will need to be held in a sample holder such as a Teflon bag. Consequently, the sample mass is unlikely to distribute itself into a regular shape with a uniform surface; measuring the areal density and thickness, or the average pile density, of these non-uniform samples then becomes extremely challenging. For these samples, accurately quantifying the induced (n, γ) reaction rate, for example, from deexcitation via γ-ray emission, may become complicated. This is especially true for high-density materials with low-to-moderate neutron-absorption cross sections, for example, tungsten, since neutron self-shielding and γ-ray absorption within the sample itself is significant and large corrections are needed. Regular geometries may be modeled rather well using particle-transport simulation toolkits such as MCNP6 [1] and GEANT4 [2]. However, insufficient knowledge of the geometric distribution of the sample, i.e. its thickness, makes it difficult to correct for attenuation in a robust and reliable manner and so alternative procedures must be developed. Some examples of methodologies that have previously been adopted to address this problem include: (i) Measuring neutron-fluence rates in Prompt Gamma Activation Analysis (PGAA), where the irradiated sample is held *in* and *out* of beam, to determine relative self-shielding factors and establish the average pile density of the sample [3]; (ii) Comparing full-energy photopeaks from ideally-thin calibration standards to the same transitions from *thick* samples to establish the γ-ray energy-dependent (E_γ) correction factors for neutron self shielding and photoattenuation [4]; (iii) Semi-quantitative Monte Carlo simulations to reproduce measured γ-ray intensity maps by iteratively adjusting neutron self absorption and photoattenuation correction factors to minimize residuals between measurement and simulation [5].

Indeed, if self-attenuation processes are not handled accurately, this can lead to misleading partial γ-ray production cross sections (σ_γ) for samples measured using PGAA setups [6,7]. This problem was highlighted recently in a study of the tungsten isotopes [8] where the new σ_γ values were found to differ considerably from those in the current Evaluated Gamma-ray Activation File (EGAF) [9,10] repository owing to neutron-attenuation and γ-ray self-absorption considerations. In this paper, we present a method for determining the *effective thickness* of a non-uniform sample via

* Corresponding author.
E-mail address: AMHurst@lbl.gov (A.M. Hurst).

http://dx.doi.org/10.1016/j.nimb.2015.09.003
0168-583X/

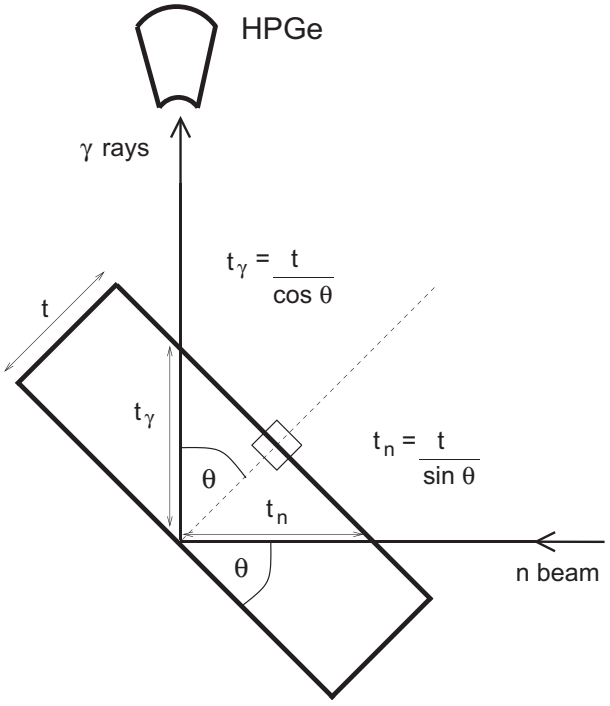

Fig. 1. Schematic illustrating the basic setup of the PGAA facility at the BRR. The sample, represented as a rectangle of thickness t, is at an angle $\theta = 30^\circ$ relative to the incident neutron-beam direction and viewed by a High-Purity Germanium (HPGe) detector mounted perpendicular to the beam direction and located ~23.5 cm from the sample. The overall exponential attenuation factor may be expressed as a linear combination of axis-resolved γ-ray and neutron-attenuation coefficients: $\exp[-(\mu_\gamma t_\gamma + \mu_n t_n)] = \exp\left[-\left(\frac{\mu_\gamma}{\cos\theta} + \frac{\mu_n}{\sin\theta}\right)t\right]$ [18].

radiative capture through exposure to a flux of near-thermal neutrons. Here, we define the effective thickness as the mean thickness *seen* by the neutrons and γ rays in an equivalent planar geometry corresponding to a homogeneous sample of the same material. As a validation of the present methodology, we also compare our results to those obtained using a suitably-thin reference calibration standard, similar to the procedure outlined in Ref. [4].

2. Method

A series of *near-thermal* ($T = 120$ K) neutron-capture measurements using isotopically-enriched and natural samples of tungsten oxide (WO_2) powders have recently been carried out [8] at the 10-MW Budapest Research Reactor (BRR) [11–16]. This work employed the PGAA setup [6,7] to measure absolute neutron-capture partial γ-ray production cross sections in tungsten isotopes produced via the radiative (n,γ) reaction with samples of enriched ^{182,183,186}W and ^{nat}W. Prompt γ-ray spectra were collected and analyzed offline using the γ-ray spectroscopy software package HYPERMET-PC [17]. Full details of the experimental setup and corresponding results are published elsewhere [8]. To obtain these precise cross sections, however, requires accurate knowledge of the *effective* sample thickness exposed to the neutron beam during irradiation. Samples that are not ideally thin, such as the high-density tungsten samples ($\rho(W) = 19.25$ g/cm^3, $\rho(WO_2) = 10.8$ g/cm^3) used in this work, are not fully transparent to neutrons and γ rays. Furthermore, because the distribution of the neutron beam is generally not spatially uniform, and in practice the beam aperture is often smaller than the actual volume of the bulk sample material, the irradiated sample may not be fully illuminated by the neutron beam. Additionally, the partial illumination zone of the sample may not be in full view of a collimated γ-ray detector. These considerations may, thus, contribute significantly to the effective sample thickness deduced from the measured peak areas in PGAA, appropriately corrected for neutron self shielding and γ-ray self absorption due to attenuation within the observed illumination zone of the sample itself.

In Section 2.1 and 2.2, respectively, we first outline the theoretical formalism governing the self-attenuation processes, and then describe how this information can be used to experimentally infer the effective thickness of the irradiated sample.

2.1. Self-attenuation correction

In general, scattered photons will emerge from an irradiated sample with a diminished photon intensity I according to the exponential-attenuation law

$$I = I_0 e^{-\mu x}, \tag{1}$$

where I_0 represents the *true* unattenuated photon intensity, x is the sample thickness, and μ is a coefficient describing the linear combination of neutron- (μ_n) and γ-ray (μ_γ) attenuation coefficients for a given sample i.e. $\mu = \mu_\gamma + \mu_n$. The angle θ of the sample holder relative to the incident beam direction, depicted by the geometry in Fig. 1, must also be taken into account in determining the overall attenuation coefficient, thus

$$\mu = \frac{\mu_\gamma}{\cos\theta} + \frac{\mu_n}{\sin\theta}. \tag{2}$$

This angle has been measured to be 30° at the BRR. The analytic form of the γ-ray energy-dependent attenuation factors [18] may then be obtained from the numerical integration of Eq. (1) over the sample thickness t

$$\frac{I}{I_0} = \int_{x=0}^{x=t} e^{-\left(\frac{\mu_\gamma}{\cos\theta}+\frac{\mu_n}{\sin\theta}\right)x} \cdot dx = \frac{1}{\left(\frac{\mu_\gamma}{\cos\theta}+\frac{\mu_n}{\sin\theta}\right)} \cdot \left[1 - e^{-\left(\frac{\mu_\gamma}{\cos\theta}+\frac{\mu_n}{\sin\theta}\right)t}\right]. \tag{3}$$

In this work, we derived the γ-ray energy dependent μ_γ values from XMuDat [19], a database of mass-attenuation coefficients, μ_γ/ρ, generated according to prescriptions outlined in Refs. [20,21]. Thus, for a natural sample of mono-elemental composition $\mu_\gamma = (\mu_\gamma/\rho)\rho$, where ρ is the sample density. For compounds, however, we must introduce a weighting factor w_i to account for the constituent elements in the compound

$$w_i = \frac{A_i}{M} \quad \text{where} \quad M = \sum_i^j A_i. \tag{4}$$

Here, A_i is atomic mass of element i and M is the total stoichiometric mass of the compound. The γ attenuation coefficients for a compound sample may then be deduced using the expression

$$\mu_{\gamma_x} = \left(\sum_i^j \frac{\mu_{\gamma_i}}{\rho_i} w_i\right)\rho_x, \tag{5}$$

where ρ_x is the measured density of the compound sample, and the summation is performed over all constituent elements i in the compound. The authors of the XMuDat database claim a precision of 5% for the absorption data, so this was adopted as a conservative estimate to derive Δ_{μ_γ}, the uncertainty in μ_γ. For thermal-neutron temperatures and lower, the neutron-attenuation coefficients may be computed from the neutron-absorption cross sections σ_{nabs} listed in Ref. [22] according to

$$\mu_{n_x} = N_A b \frac{T_0}{T} \rho_x \sum_i^j \frac{\sigma_{\mathrm{nabs},i}}{A_i} w_i, \tag{6}$$

where $N_A = 6.022 \times 10^{23}$ is the Avogadro constant, the conversion factor $b = 1 \times 10^{-24}$ cm^2, $T_0 = 293$ K represents the *true* thermal-neutron temperature, $T = 120$ K is the assumed *near-thermal* temperature of the BRR neutron beam. Clearly, for samples of mono-elemental composition $w_i = 1$, in Eq. (6) above, and ρ_x is simply replaced by ρ_i. The uncertainty in μ_n, written as Δ_{μ_n}, is determined by propagating through the uncertainty on σ_{nabs} alone, with all other terms in Eq. (6) treated as constants. This expression is strictly valid for a given neutron-beam temperature rather than a distribution. In practice, the neutrons will gain energy as they traverse the bulk volume of the sample, and for certain materials, a Monte Carlo calculation may be required to account for neutron thermalization over a disparate temperature range. However, for the tungsten oxide powders measured in this work, lowering the beam temperature by as much as 50 K only induces a change of the order of $\sim 1\%$ at 77 keV in the overall attenuation.

Assuming μ_γ and μ_n to be independent variables, the overall uncertainty on the attenuation factor I/I_0 is then derived using the law of combination of errors

$$\Delta^2_{I/I_0} = \left[\frac{\partial}{\partial \mu_\gamma}\left(\frac{I}{I_0}\right)\right]^2 \Delta^2_{\mu_\gamma} + \left[\frac{\partial}{\partial \mu_n}\left(\frac{I}{I_0}\right)\right]^2 \Delta^2_{\mu_n}. \tag{7}$$

Appropriate error propagation and differentiating I/I_0 (Eq. (3)) with respect to μ_γ and μ_n, independently, yields the following expression quantifying the variance in I/I_0 from which the overall uncertainty may be deduced

$$\Delta^2_{I/I_0} = \left[\frac{1}{\frac{\mu_\gamma}{\cos\theta} + \frac{\mu_n}{\sin\theta}}\left(te^{-\left(\frac{\mu_\gamma}{\cos\theta}+\frac{\mu_n}{\sin\theta}\right)t} - \frac{I}{I_0}\right)\right]^2 \times \left(\frac{\Delta^2_{\mu_\gamma}}{\cos^2\theta} + \frac{\Delta^2_{\mu_n}}{\sin^2\theta}\right). \tag{8}$$

2.2. Standardization and determination of the effective sample thickness

To establish the effective target thickness of the thick high-density tungsten samples measured in this work, a set of absolute neutron-capture partial γ-ray production cross sections is required for comparison. Adopting comparator γ-ray transitions, whose cross sections are well known, permits use of an internal-standardization procedure, outlined in detail in Ref. [23]. In this procedure, the observed γ-ray intensities may be normalized by scaling to the well-known comparator transitions observed in the same capture-γ spectrum. For comparative purposes here, we used strong γ lines in ^{187}W that were extracted from a previous thin-sample measurement of a low-density hydrated tungstic acid (H_2WO_4) compound of natural composition [8]. In that measurement, the absolute cross sections for the ^{187}W γ lines, listed in Table 1, were extracted via internal standardization to the 2223-keV transition in hydrogen which has a well-known partial γ-ray production cross section $\sigma_\gamma(2223\ \mathrm{keV}) = 0.3326(7)$ b [23], and taking into account the stoichiometric ratio of H : W. The lack of any strong *s*-wave resonances near the thermal-neutron point at 25.3 meV in tungsten renders applicable a pure $1/v$ dependence on the observed cross section near and below thermal-neutron energies (E_n). Under these circumstances, the cross section may be represented as shown in Ref. [24], accordingly:

$$\sigma_\gamma(E_n; v) = \sigma_0 \sqrt{\left(\frac{E_0}{E_n}\right)} = \sigma_0\left(\frac{v_0}{v}\right), \tag{9}$$

where σ_0 is the total radiative thermal neutron-capture cross section, $v_0 = 2200$ m/s is the thermal neutron velocity, and $E_0 = 25.3$ meV. It follows, therefore, that

$$\sigma_\gamma(E_n) \propto \frac{1}{v} \quad \forall \quad E_n \lesssim 25.3\ \mathrm{meV}. \tag{10}$$

Also, since $(T_0/T) = \sqrt{(E_0/E)}$, at our assumed average beam temperature $T = 120$ K, the $1/v$ law implies a corresponding neutron-beam energy centered around 4.2 meV. Thus, although Eqs. 9 and 10 are rigorously defined for monoenergetic neutrons [24], our measurement concerns a distribution of neutrons centered on ~ 4.2 meV. However, because both tungsten and hydrogen obey the $1/v$ law (i.e. Eqs. 9 and 10 are valid), moreover since σ_γ(W) are deduced relative to σ_γ(H), it follows that any correction for the neutron-beam energy cancels.

The absolute cross sections, σ^S_γ, of Table 1 [8] were adopted for standardization purposes since they cover the complete energy range of interest: from below 100 keV, where γ-ray self absorption is significant, to several MeV, where absorption is negligible. In general, the measured peak areas A_γ observed in the capture-γ spectrum are related to their corresponding transition cross sections according to the expression

$$A_\gamma = \sigma_\gamma \frac{mN_A}{M} \theta \epsilon_\gamma(E_\gamma) \frac{I(E_\gamma)}{I_0} \phi \tau g_W(T), \tag{11}$$

where m (the sample mass), N_A, and M are described in Section 2.1, θ is the isotopic abundance, ϕ is the neutron flux, τ is the data-acquisition deadtime-corrected irradiation period, and $\epsilon_\gamma(E_\gamma)$

Table 1
Transition energies (E_γ) from ^{186}W$(n,\gamma)^{187}$W and their corresponding absolute neutron-capture partial γ-ray production cross sections (σ^S_γ) obtained from a standardized $H_2WO_4(n,\gamma)$ measurement [8]. Standardization energies and cross sections from ^{182}W$(n,\gamma)^{183}$W are also presented. The transitions are indexed (i) in order of ascending E_γ. The efficiency-corrected peak areas, denoted A'_γ, were measured using enriched powdered samples of ^{186}W (99.65(3)%) and ^{182}W (92.7(9)%); A^c_γ represent the same peak areas corrected for γ-ray absorption and neutron self shielding assuming the deduced effective sample thicknesses of 0.077 mm and 0.042 mm, respectively. In the final column the proportionality constant, $R_i(E_{\gamma_i})$, relating σ^S_γ and A^c_γ is listed. See text for details.

Sample	E_γ [keV]	i	σ^S_γ [b]	A'_γ [cnt]	A^c_γ [cnt]	$R_i(E_{\gamma_i})$ [b · cnt^{-1}]
^{186}W	77.30(5)	1	0.234(4)	13361(321)	25950(623)	9.02×10^{-6}(27)
	145.84(5)	2	1.344(13)	124860(5619)	146941(6612)	9.15×10^{-6}(42)
	273.12(5)	3	0.380(4)	38868(3848)	41078(4066)	9.25×10^{-6}(92)
	5261.67(9)	4	0.653(9)	70901(1205)	72449(1231)	9.01×10^{-6}(20)
^{182}W	98.90(1)	1	0.0906(32)	11602(174)	14375(215)	6.30×10^{-6}(24)
	162.11(1)	2	0.2605(72)	37534(450)	40356(483)	6.45×10^{-6}(19)
	291.57(1)	3	0.0665(25)	10358(124)	10644(127)	6.25×10^{-6}(25)
	1100.39(3)	4	0.0334(14)	5282(137)	5349(138)	6.24×10^{-6}(31)
	6190.78(6)	5	0.726(10)	112700(1578)	114043(1596)	6.37×10^{-6}(13)

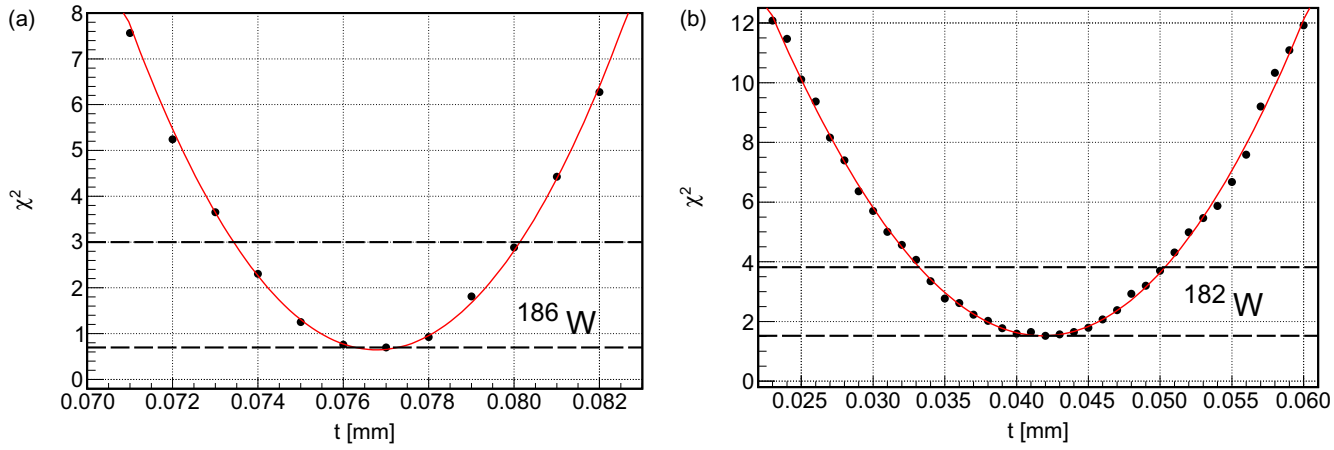

Fig. 2. Plots showing the global χ^2 distribution as a function of thickness (t) for the ^{186}W (a) and ^{182}W (b) samples measured in this work. The lower-dashed line in each plot indicates the minima of the respective distributions and corresponds to the mean effective target thickness: (a) $\chi^2_{min} \approx 0.70$ (ndf = 2) at $t = 0.077$ mm; (b) $\chi^2_{min} \approx 1.5$ (ndf = 3) at $t = 0.042$ mm. The upper-dashed line is drawn at $\chi^2_{min} + 2.3$ in each plot to illustrate the 1σ acceptable range of t values consistent with the uncertainty window (Δt) of the deduced effective target thickness.

denotes the relative γ-ray energy-dependent detection efficiency. The detection efficiency represents a total efficiency given by the product of the intrinsic-detection efficiency and the geometric efficiency describing the solid angle subtended by the detector with respect to the sample position. The temperature-dependent Westcott g factor, $g_W(T)$, is a correction factor used to describe non-$1/v$ behavior exhibited by irregular nuclides [24]; g_W is given by the ratio of the effective cross section for a pure Maxwellian spectrum at a given T to the 2200-m/s (i.e. $T = 293$ K) cross section [25]. The g_W factors for the hydrogen and tungsten isotopes considered in this study do not deviate from unity by more than 1% at $T = 120$ K or at $T = 293$ K [25], i.e. $g_W \approx 1$ and no correction to A_γ is needed. Because m, N_A, M, θ, ϕ, τ, and T are systematic quantities that contribute to the observed count rate in all γ lines, collectively they constitute a constant K, such that

$$\frac{A'_\gamma}{\sigma_\gamma} \cdot \frac{1}{I(E_\gamma)/I_0} = K, \tag{12}$$

where $A'_\gamma = A_\gamma/\epsilon_\gamma(E_\gamma)$ is the efficiency-corrected peak area. Although both ϵ_γ and the attenuation factor I/I_0 are dependent on E_γ, since the measured peak area for a given transition is directly proportional to its corresponding absolute standard cross section, it follows that the ratio of σ^S_γ to the measured peak area will be constant for any transition provided the peak areas have been appropriately corrected for these quantities. This condition may be expressed as

$$\frac{\sigma^S_{\gamma_1}(E_{\gamma_1})}{A^c_{\gamma_1}(E_{\gamma_1})} = \frac{\sigma^S_{\gamma_2}(E_{\gamma_2})}{A^c_{\gamma_2}(E_{\gamma_2})} = \frac{\sigma^S_{\gamma_3}(E_{\gamma_3})}{A^c_{\gamma_3}(E_{\gamma_3})} = \cdots \tag{13}$$

or, in general terms,

$$R_i(E_{\gamma_i}) = \frac{\sigma^S_{\gamma_i}(E_{\gamma_i})}{A^c_{\gamma_i}} = \text{const.} \tag{14}$$

where A^c_γ represents the attenuation-corrected measured peak area given by

$$A^c_\gamma = \frac{A'_\gamma}{I/I_0(t)}, \tag{15}$$

and A'_γ is the ϵ_γ-corrected attenuated peak area measured directly in the capture-γ spectrum. The effective sample thickness is then determined by treating t as an adjustable parameter in Eq. (3) and varying this quantity until the condition embodied by the ratio in Eqs. 13 and 14 converges upon a unique result. An appropriate energy-dependent attenuation correction can then be applied to the entire capture-γ spectrum. Uncertainties for all relevant quantities are determined and propagated in the standard manner; they are also listed in Table 1.

For a given sample, since the ratios $R_i(E_{\gamma_i})$ are not independent measurements but are in fact correlated, a covariance matrix $\mathbf{V}$, containing the associated uncertainties Δ_{R_i}, is needed to describe them. From the principle of maximum likelihood we know that the probability of a particular set of data is the product of the individual probabilities, and this provides a basis for the least squares method adopted in this analysis. By minimizing the exponent in the Gaussian likelihood function we may determine the global χ^2 for an assumed effective thickness t using the following expression

$$\chi^2 = \sum_{i=1}^{N}\sum_{j=1}^{N}[R_w - R_i(E_{\gamma_i})][V_{ij}^{-1}][R_w - R_j(E_{\gamma_j})], \tag{16}$$

where R_w is the expectation value at a given t determined from the weighted average of the corresponding set of $R_i(E_{\gamma_i})$ measurements. The individual (i, j) elements of an $N \times N$ covariance matrix, where N represents the maximum number of data points, are given as $V_{ij} = \Delta^2_{R_i}\delta_{ij}$ for the diagonal elements (where the Kronecker delta function $\delta_{ij} = 1$ for $i = j$, and 0 for $i \neq j$) and $V_{ij} = r_{ij}\Delta_{R_i}\Delta_{R_j}$ for the off-diagonal matrix elements, where r_{ij} is the correlation coefficient between a pair of $R_i(E_{\gamma_i})$ measurements. For each of the N data points the corresponding ratios $R_1(E_{\gamma_1})$, $R_2(E_{\gamma_2})$, …, $R_N(E_{\gamma_N})$, may be denoted $\mathbf{R}$, where $\mathbf{R}$ is a vector of N elements. Writing $\mathbf{R_w}$ also as an N-element vector then allows Eq. (16) to be conveniently recast in matrix notation as

$$\chi^2 = (\mathbf{R_w} - \mathbf{R})\mathbf{V}^{-1}(\widetilde{\mathbf{R_w}} - \widetilde{\mathbf{R}}), \tag{17}$$

where $\widetilde{\mathbf{R_w}}$ and $\widetilde{\mathbf{R}}$ represent the transposed vectors $\mathbf{R_w}$ and $\mathbf{R}$, respectively.

In this work, two parameters (P) are adjusted to minimize χ^2 to fit the N data points: t and r_{ij}. Here, r_{ij} represents an average solution. The number of degrees of freedom is given by ndf $= N - P$. For the ^{186}W and ^{182}W measurements $N = 4$ and 5, respectively, thus

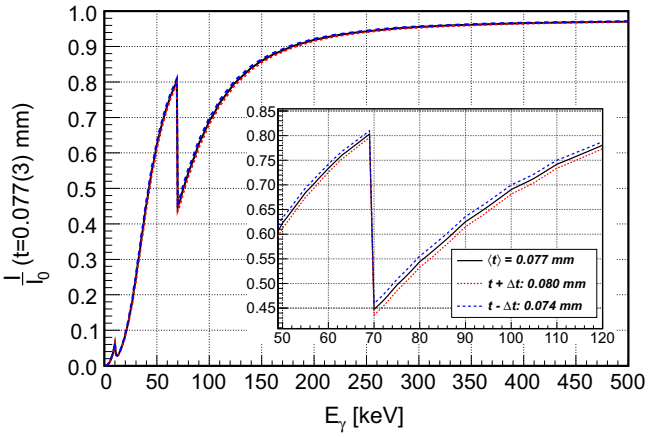

Fig. 3. The γ-ray energy-dependent attenuation factor, I/I_0, plotted as a function of E_γ for the ^{186}W sample assuming $t = 0.077(3)$ mm in Eq. (3). The curve is expanded around $E_\gamma = 50$–120 keV to reveal the upper and lower bounds of the uncertainty band (for one standard deviation). This curve provides an E_γ-dependent correction to the measured transition intensities in the capture-γ spectrum. The abrupt K-edge in tungsten is clearly visible at around 69–70 keV and corresponds to a sharp increase in μ_γ at the K-shell electron binding energy; the smaller cumulative effect of the L-I, L-II, and L-III edges is also observed in the low-energy regime spanning approximately 10–12 keV.

ndf = 2 and 3, respectively. According to Poisson statistics the reduced χ^2, i.e. χ^2/ndf, for distributions with ndf = 2 and 3 are expected to be ~ 0.35 and ~ 0.5, respectively, at the 68.3% confidence level [26]. The corresponding value of t yielding a global $\chi^2_{\min}$, at values of approximately 0.7 (^{186}W; ndf = 2) and 1.5 (^{182}W; ndf = 3), for the fit from a two-parameter adjustment may then be interpreted as the mean effective sample thickness. Its uncertainty Δt can then be extracted using the method of least squares from the range of values for $t \pm \Delta t$ satisfying the condition $\chi^2 \leqslant \chi^2_{\min} + 2.3$ [26]. Accordingly, we estimate Δt using

$$\Delta t = \frac{1}{2}\left[t_>(\chi^2_{\min} + 2.3) - t_<(\chi^2_{\min} + 2.3)\right], \tag{18}$$

where $t_>$ and $t_<$ are the interpolated values of t at $\chi^2_{\min} + 2.3$, with $t_> > t$ and $t_< < t$.

3. Results

To illustrate the procedure for determination of the effective thickness t, we present results from an (n, γ) measurement for a 169-mg powder sample of $^{186}WO_2$ (99.65(3)% enrichment) irradiated for a period of 2.03 h to induce prompt radioactivity in the ^{187}W compound nucleus [8]. Alongside the standardization-transition energies and cross sections listed in Table 1 are the corresponding ϵ_γ-corrected attenuated peak areas, A'_γ. Using this data, we iteratively step through values of t over a suitable range of thicknesses to calculate $A^c_{\gamma_i}$ (Eq. (15)) to find a statistically consistent $R_i(E_{\gamma_i})$ (Eq. (14)) data set. Simultaneously, we adjust r_{ij} between 0 and 1 to minimize the χ^2 function in Eq. (17). Fig. 2(a) shows the global χ^2 distribution plotted as a function of t and reveals a tungsten effective sample thickness $t = 0.077$ mm (equivalent to 0.16 mm for WO_2), assuming an overall average correlation coefficient $r_{ij} = 0.82$, can reproduce $\chi^2_{\min} = 0.70$ i.e. the global χ^2 expectation value for a minimization based on ndf = 2. The corresponding results for $A^c_{\gamma_i}$ and $R_i(E_{\gamma_i})$ at $t = 0.077$ mm are also summarized in Table 1, from which an average $R_w = 9.04 \times 10^{-6}$ b · cnt^{-1} is determined. The elements of the covariance matrix supporting this result may be written as a product of the correlation coefficient and the associated $R_i(E_{\gamma_i})$ uncertainty products, Δ_{R_i} from Table 1. Because $N = 4$, the general form of the 4×4 covariance matrix may be represented as

$$V = \begin{pmatrix} r_{11}\Delta_{R_1}\Delta_{R_1} & r_{12}\Delta_{R_1}\Delta_{R_2} & r_{13}\Delta_{R_1}\Delta_{R_3} & r_{14}\Delta_{R_1}\Delta_{R_4} \\ r_{21}\Delta_{R_2}\Delta_{R_1} & r_{22}\Delta_{R_2}\Delta_{R_2} & r_{23}\Delta_{R_2}\Delta_{R_3} & r_{24}\Delta_{R_2}\Delta_{R_4} \\ r_{31}\Delta_{R_3}\Delta_{R_1} & r_{32}\Delta_{R_3}\Delta_{R_2} & r_{33}\Delta_{R_3}\Delta_{R_3} & r_{34}\Delta_{R_3}\Delta_{R_4} \\ r_{41}\Delta_{R_4}\Delta_{R_1} & r_{42}\Delta_{R_4}\Delta_{R_2} & r_{43}\Delta_{R_4}\Delta_{R_3} & r_{44}\Delta_{R_4}\Delta_{R_4} \end{pmatrix},$$

where, for the diagonal matrix elements $r_{ij} = 1$ (see Section 2.2), and for all off-diagonal elements $r_{ij} = 0.82$. Thus, using these values for r_{ij} together with the corresponding indexed uncertainties from the final column of Table 1 yields

$$V = \begin{pmatrix} [1.00 \times 0.27 \times 0.27] & \cdots & [0.82 \times 0.27 \times 0.20] \\ [0.82 \times 0.42 \times 0.27] & \cdots & [0.82 \times 0.42 \times 0.20] \\ [0.82 \times 0.92 \times 0.27] & \cdots & [0.82 \times 0.92 \times 0.20] \\ [0.82 \times 0.20 \times 0.27] & \cdots & [1.00 \times 0.20 \times 0.20] \end{pmatrix}.$$

For clarity, we have factored through the 10^{-6} common denominator associated with all $R_i(E_{\gamma_i})$ and Δ_{R_i} values of Table 1, thus simplifying the χ^2 calculation.

The overall uncertainty on the target thickness is extracted from the global χ^2 distribution and interpolating the range of t consistent with $\chi^2 \leqslant \chi^2_{\min} + 2.3 \lesssim 3$. Fig. 2(a) shows that values of t between approximately 0.0734 and 0.0801 mm (3 sf) satisfy this criterion window of $\chi^2 \lesssim 3$. Hence, from Eq. (18) we report an estimate for $\Delta t = \pm 0.003$ mm (3 dp). Our result for the *effective target thickness* of the inhomogeneous powder sample, therefore, describes the equivalent planar thickness of the tungsten sample based on the measured apparent overall self attenuation within the sample. The one-standard-deviation γ-ray energy-dependent attenuation correction, applicable to the observed γ-ray intensities measured in the (n, γ) capture spectrum [8], corresponding to an effective thickness $t = 0.077(3)$ mm is shown in Fig. 3. From a similar analysis carried out on a 274-mg $^{182}WO_2$ sample (92.7(9)% enrichment) irradiated for 2.46 h, we established the global $\chi^2_{\min} = 1.5$ (the expectation value based on ndf = 3) using $r_{ij} = 0.60$ and $R_w = 6.35 \times 10^{-6}$ b · cnt^{-1} to extract an effective sample thickness $t = 0.042(8)$ mm for ^{182}W (equivalent to 0.087 mm for WO_2) as shown in Fig. 2(b).

As a consistency check, the overall attenuation factors may also be deduced experimentally by comparing the *attenuated* partial γ-ray production cross sections from the *thick* high-density ^{186}W and ^{182}W measurements, referred to as $\sigma^{\mathrm{T}}_\gamma$, to the same transitions from the reference standard with known absolute cross sections, $\sigma^{\mathrm{S}}_\gamma$. A similar procedure is described in Ref. [4]. The attenuated $\sigma^{\mathrm{T}}_\gamma$ values are also deduced via the internal-standardization procedure (see Section 2.2 and references therein): for the ^{186}W sample we scaled to the high-energy comparator line in ^{187}W at 5261.68 keV; for the ^{182}W sample we used the 6190.78-keV line in ^{183}W. Both high-energy primary γ rays are subject to negligible absorption. Because the thick-sample cross sections, $\sigma^{\mathrm{T}}_\gamma$, have not been corrected for self attenuation, and $\sigma^{\mathrm{S}}_\gamma$ represents the ideal standard for a given transition, the experimental attenuation factor, $(I/I_0)_{\mathrm{exp}}$, may be defined by the following ratio

$$\left(\frac{I}{I_0}\right)_{\mathrm{exp}} = \frac{\sigma^{\mathrm{T}}_\gamma}{\sigma^{\mathrm{S}}_\gamma}. \tag{19}$$

Table 2
Standard cross sections, σ_γ^S, in $^{186}W(n,\gamma)^{187}W$ and $^{182}W(n,\gamma)^{183}W$ are derived from the H_2WO_4 normalization measurement [8] and the attenuated cross sections, σ_γ^T, are from the thick-sample measurements using enriched ^{186}W and ^{182}W, respectively. Cross sections are corrected for isotopic abundances: ^{186}W (28.43%) and ^{182}W (26.50%) [27]. The experimental attenuation factors $(I/I_0)_{exp}$ were deduced from the ratio $\sigma_\gamma^T/\sigma_\gamma^S$ (Eq. (19)) and compared to the theoretical values I/I_0 (Eq. (3)) using effective thicknesses of 0.077 mm (^{186}W) and 0.042 mm (^{182}W), assuming: (1) both γ-ray absorption and neutron self shielding; (2) γ-ray absorption only. Uncertainties are smaller in the first case owing to the overall non-linearity represented by the combination μ_γ and μ_n according to the functional form of Eq. (8).

Sample	E_γ [keV]	σ_γ^S [b]	σ_γ^T [b]	$\left(\frac{I}{I_0}\right)_{exp}$	$\left(\frac{I}{I_0}\right)_{<\mu_\gamma+\mu_n>}$ [1]	$\left(\frac{I}{I_0}\right)_{<\mu_\gamma>}$ [2]
^{186}W	77.39(3)	0.823(14)	0.433(14)	0.526(19)	0.514(25)	0.522(26)
	145.79(3)	4.727(46)	4.05(20)	0.856(44)	0.849(37)	0.867(43)
	273.10(5)	1.337(14)	1.26(13)	0.942(96)	0.943(30)	0.963(48)
	5261.68(6)	2.297(32)	2.297(64)	1.000(31)	0.975(15)	0.997(49)
^{182}W	98.90(1)	0.342(12)	0.282(7)	0.825(36)	0.806(38)	0.815(41)
	162.11(1)	0.983(27)	0.912(21)	0.928(33)	0.928(39)	0.939(47)
	291.57(1)	0.251(9)	0.252(6)	1.003(44)	0.973(28)	0.985(49)
	1100.39(3)	0.126(5)	0.128(4)	1.019(54)	0.985(16)	0.997(50)
	6190.78(6)	2.740(38)	2.740(66)	1.000(28)	0.986(15)	0.998(50)

[1] Calculated using Eq. (3) assuming both γ-ray and neutron attenuation.
[2] Calculated using Eq. (3) assuming γ-ray attenuation only.

Clearly, for lower-energy transitions the observed attenuation is more apparent and although $\sigma_\gamma^T < \sigma_\gamma^S$ for all transitions, σ_γ^T asymptotically reaches σ_γ^S as E_γ increases beyond $\gtrsim 300$ keV (where $I/I_0 \to 1$). Presented in Table 2 are the standardized thick-sample cross sections, corrected for the respective isotopic abundances of ^{186}W (28.43%) and ^{182}W (26.50%) [27], and the corresponding experimental attenuation factors. The effective sample thicknesses extracted from the covariance analyses may then be compared to the observed experimental values given by Eq. (19) for each E_γ. As shown in Table 2, the theoretical values for I/I_0, assuming $t = 0.077$ mm for the ^{186}W sample and $t = 0.042$ mm for ^{182}W sample, compare favorably with the experimentally-deduced values for each E_γ. Remarkable consistency is achieved assuming: (i) both γ-ray self absorption and neutron self shielding (Eq. (3)); (ii) γ-ray self absorption alone (Eq. (3) without the μ_n dependence). In the thick-sample approximation, the irradiated sample absorbs all incident neutrons allowing the γ-ray absorption to be treated independently. Our results in this case reveal very little difference in the calculation of $I/I_0(\mu_\gamma, \mu_n)$ and $I/I_0(\mu_\gamma)$ at the assumed sample thicknesses and both sets of calculations are in excellent agreement with the experimentally-deduced attenuations. This agreement is reinforced in Fig. 4 which shows excellent consistency between calculated and experimental attenuation factors, not only for the transitions used in deriving the effective sample thickness (red data points), but also for other prominent transitions (black data points) that may be used for comparison between the standard (H_2WO_4) and enriched thick-target (n, γ) spectra. This observation provides a useful verification of the adopted method for the determination of the effective sample thickness.

4. Conclusions

A capability has been demonstrated to precisely determine effective sample thicknesses for irregular geometries with non-uniform areal densities through radiative capture. This technique is predicated on quantifying the γ-ray absorption observed in low-energy transitions by comparison to known absolute partial γ-ray production cross sections, and has been experimentally verified through neutron-beam (n, γ) measurements performed with the PGAA setup at the BRR. We have successfully illustrated this concept to a precision of better than 4% for a 0.077(3)-mm measurement of the tungsten-equivalent effective sample thickness for an enriched $^{186}WO_2$ powdered sample, and we have also measured a tungsten-equivalent effective sample thickness of 0.042(8) mm for an enriched $^{182}WO_2$ powdered sample. The level of precision attained may be explained by the sensitivity of the γ-ray yield for low-energy transitions with respect to the assumed sample thickness. In the case of ^{186}W, the strong well-resolved low-energy transition at ~ 77 keV provides enhanced sensitivity for this adopted methodology.

For materials, such as tungsten, with low-to-moderate neutron-capture cross sections, neutrons are more likely to penetrate deeper into the sample, and so capture-reaction radioactivity is likely to be induced from deeper within the bulk-sample volume. Consequently, the transmission path through which the γ rays must traverse, on average, is likely to represent the mean thickness of the irradiated sample. Because tungsten is also a high-ρ density material, the probability of complete photoelectric absorption within the sample is also high leading to large corrections, particularly for the lower-energy ($\lesssim 300$ keV) transitions that are subject to higher degrees of γ-ray self absorption. The amount of overall attenuation, therefore, provides a measure of the apparent, effective, thickness of the sample volume illuminated by the neutron beam. In general, this measured effective thickness is likely to be somewhat less than the *true* thickness represented by the entirety of the bulk sample material, and the amount of absorption and self shielding from an integration over the true thickness may constitute an over estimate of the correction factor. Furthermore, γ-ray transmission through samples with high neutron-capture cross sections, or low-ρ materials, is far less likely to be impeded to a measurable extent. However, future measurements are needed to help understand the limitations, and useful implementations, of this technique.

Acknowledgements

This work was performed under the auspices of the University of California, supported by the Director, Office of Science, Office of Basic Energy Sciences, of the U.S. Department of Energy at the Lawrence Berkeley National Laboratory under Contract DE-AC02-05CH11231, and by the U.S. Department of Energy by the Lawrence Livermore National Laboratory under Contract DE-AC52-07NA27344. The access to the Budapest PGAA facility was financially supported by the NAP VENEUS08 grant under Contract OMFB-00184/2006. The operations staff at the Budapest Research Reactor are gratefully acknowledged. A.H. thanks Dr. W. Younes for insightful physics discussions.

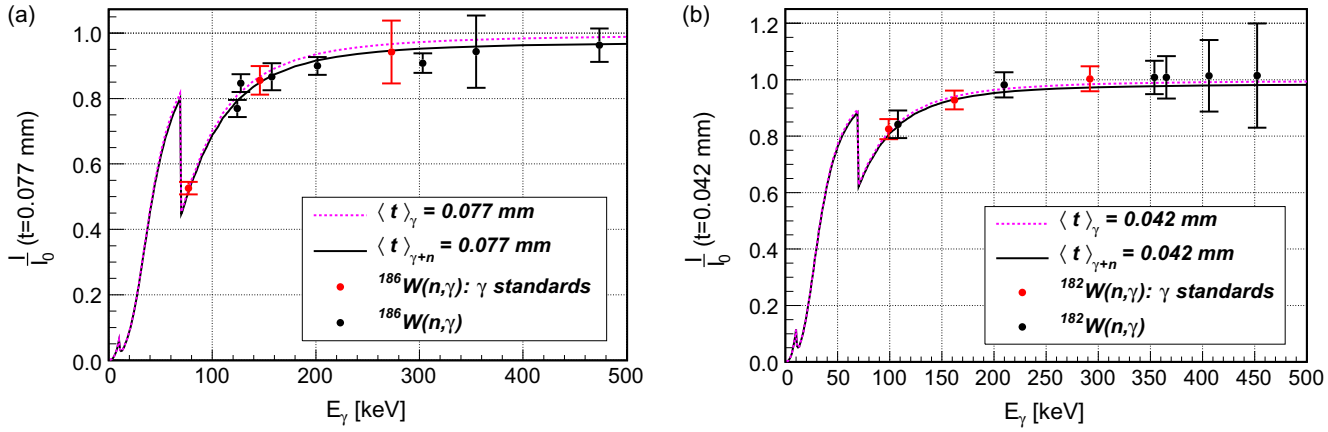

Fig. 4. The γ-ray energy-dependent attenuation factor, I/I_0, plotted as a function of E_γ for energies up to 500 keV, assuming: (a) $t = 0.077$ mm (^{186}W); (b) $t = 0.042$ mm (^{182}W). The solid-black curve corresponds to I/I_0 as a function of both μ_γ and μ_n, whereas the dashed-magenta curve neglects the μ_n dependence i.e. I/I_0 as a function of μ_γ alone. The data points show the experimentally-deduced attenuation factors for individual γ-ray transitions using Eq. (19): the red points correspond to transitions used to deduce the ^{186}W and ^{182}W sample thicknesses; the black data points were not used in the derivation of the sample thicknesses but only for comparison.

References

[1] J. T. Goorley, et al., Initial MCNP6 Release Overview – MCNP6 version 1.0, LA-UR-13-22934 (2013); <https://mcnp.lanl.gov/>.
[2] S. Agostinelli et al., Nucl. Instrum. Methods Phys. Res., Sect. A 506 (2003) 250.
[3] M. Blaauw, T. Belgya, J. Radioanal. Nucl. Chem. 265 (2005) 257.
[4] A. Borella et al., J. Radioanal. Nucl. Chem. 265 (2005) 267.
[5] Z. Kis, T. Belgya, L. Szentmiklósi, Nucl. Instrum. Methods Phys. Res., Sect. A 638 (2011) 143.
[6] Zs. Révay et al., Nucl. Instrum. Methods Phys. Res., Sect. B 213 (2004) 385.
[7] L. Szentmiklósi et al., J. Radioanal. Nucl. Chem. 286 (2010) 501.
[8] A.M. Hurst et al., Phys. Rev. C 89 (2014) 014606.
[9] R.B. Firestone, Database of Prompt Gamma Rays from Slow Neutron Capture for Elemental Analysis, International Atomic Energy Agency, Vienna, 2007. Chap. Adopted Database and User Tables, p. 73, <https://www-nds.iaea.org/pgaa/egaf.html>.
[10] Zs. Révay, R.B. Firestone, T. Belgya, G.L. Molnár, Handbook of Prompt Gamma Activation Analysis, Kluwer Academic Publishers, The Netherlands, 2004. Chap. Prompt Gamma-Ray Spectrum Catalog, p. 173.
[11] T. Belgya, et al., in: Proc. 9th International Symposium on Capture Gamma-Ray Spectroscopy and Related Topics, Springer Verlag, Budapest, Hungary, 1997, p. 826.
[12] L. Rosta et al., Physica B 234–236 (1997) 1196.
[13] L. Rosta, Appl. Phys. A 74 (2002) S52.
[14] L. Rosta, T. Grósz, T. Hargitai, Appl. Phys. A 74 (2002) S240.
[15] T. Belgya, Phys. Proc. 31 (2012) 99.
[16] T. Belgya, Z. Kis, L. Szentmiklósi, Nucl. Data Sheets 119 (2014) 419.
[17] B. Fazekas et al., J. Radioanal. Nucl. Chem. 215 (1997) 271.
[18] Zs. Révay, Anal. Chem. 81 (2009) 6851.
[19] R. Nowotny, XMuDat: Photon attenuation data on PC, IAEA-NDS-195, Version 1.0.1, August 1998, <https://www-nds.iaea.org/publications/iaea-nds/iaea-nds-0195.htm>.
[20] J.H. Hubbel, S.M. Seltzer, Tables of X-ray Mass Attenuation Coefficients and Mass Energy-Absorption Coefficients 1 keV to 20 MeV for Elements $Z = 1$ to 92 and 48 Additional Substances of Dosimetric Interest, NISTIR 5632, 1995, <http://www.nist.gov/pml/data/xraycoef/index.cfm/>.
[21] J.M. Boone, A.E. Chavez, Med. Phys. 23 (12) (1997) 1996.
[22] S.F. Mughabghab, Atlas of Neutron Resonances: Resonance Parameters and Thermal Cross Sections $Z = 1$–100, fifth ed., Elsevier, BV, New York, 2006.
[23] Zs. Révay, G.L. Molnár, Radiochim. Acta 91 (2003) 361.
[24] Zs. Révay, T. Belgya, Handbook of Prompt Gamma Activation Analysis, Kluwer Academic Publishers, The Netherlands, 2004. Chap. Principles of the PGAA method, p. 1.
[25] H.D. Choi, T. Trkov, Database of Prompt Gamma Rays from Slow Neutron Capture for Elemental Analysis, International Atomic Energy Agency, Vienna, 2007. Chap. Nomenclature, Westcott g_W Factors and Neutron Spectral Shape Dependent Formalism, p. 5.
[26] J. Beringer et al., Particle data group, Phys. Rev. D 86 (2012) 390–401. 010001, G. Cowan, Statistics.
[27] M. Berglund, M. Wiesser, Pure Appl. Chem. 83 (2011) 397.